

pubs.acs.org/JPCA Article

Wave Function Based Analysis of Dynamics versus Yield of Free Triplets in Intramolecular Singlet Fission

Published as part of The Journal of Physical Chemistry virtual special issue "Josef Michl Festschrift".

Rafi Chesler, Souratosh Khan, and Sumit Mazumdar*



Cite This: J. Phys. Chem. A 2020, 124, 10091-10099



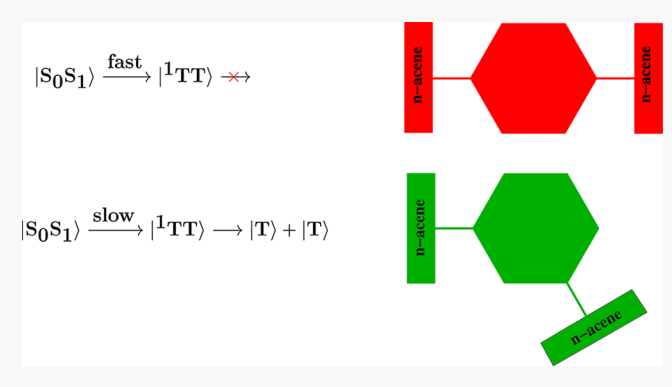
ACCESS

Metrics & More

Article Recommendations

Supporting Information

ABSTRACT: Experiments in several intramolecular singlet fission materials have indicated that the triplet—triplet spin biexciton has a much longer lifetime than believed until recently, opening up loss mechanisms that can annihilate the biexciton prior to its dissociation to free triplets. We have performed many-body calculations of excited state wave functions of hypothetical phenylene-linked anthracene molecules to better understand linker-dependent behavior of dimers of larger acenes being investigated as potential singlet fission candidates. The calculations reveal unanticipated features that we show carry over to the real covalently linked pentacene dimers. Dissociation of the correlated triplet—triplet spin biexciton and free triplet generation may be difficult in acene dimers where the formation of the triplet—triplet



spin biexciton is truly ultrafast. Conversely, relatively slower biexciton formation may indicate smaller spin biexciton binding energy and greater yield of free triplets. Currently available experimental results appear to support this conclusion. Whether or not the two distinct behaviors are consequences of distinct mechanisms of triplet—triplet generation from the optical singlet is an interesting theoretical question.

■ INTRODUCTION

Singlet-fission (SF), a spin-allowed multichromophore process in which two spin-triplet excitons are generated from a single optically allowed spin-singlet exciton, is of strong current interest, ^{1,2} as successful implementation of SF can double the performance of organic solar cells.^{3–5} While initial research focused mostly on molecular systems that exhibit intermolecular SF (xSF), interest has more recently been extended to covalently linked dimers and oligomers of chromophore molecules that exhibit intramolecular SF (iSF).^{6–18} The work reported here is primarily concerned with iSF in covalently liked dimers of chromophore molecules, although the broad conclusion we arrive at applies also to xSF.

In what follows, we use the ket notation to denote quantum-mechanical eigenstates, which are understood to be superpositions of many-electron configurations. The absolute ground state is written as $|S_0S_0\rangle$, the lowest optical singlet and triplet as $|S_0S_1\rangle$ and $|S_0T_1\rangle$, respectively (with the understanding that the actual symmetry-adapted eigenstates include configurations in which the molecules in their ground and excited states are switched). It is broadly accepted that SF is a two-step process in which $|S_0S_1\rangle$ first undergoes internal conversion to a bound triplet—triplet spin-singlet spin-biexciton, $|^1TT\rangle$. Free triplets are generated from

dissociation of $|^{1}TT\rangle$. Based on transient absorption (TA) studies, it was believed until recently that free triplets T_{1} were being generated in ultrafast time scales (from hundreds of fs to ps). It is now realized that the earlier experiments were mostly detecting not free triplets but the bound $|^{1}TT\rangle$, $|^{19-27}$ whose lifetime can extend from nano- to microseconds. Direct decay of the $|^{1}TT\rangle$ into $|S_{0}S_{0}\rangle$ or triplet—triplet annihilation are both possible over such a long period, indicating that actual implementation of SF in photovoltaics will require understanding both steps of SF equally well. Theoretical research on SF has until now mostly focused on step 1, as determining an accurate description of $|^{1}TT\rangle$ continues to be a formidable problem within traditional quantum chemical approaches.

The |¹TT⟩ is a double excitation from the Hartree–Fock (HF) ground state in the molecular orbital (MO) representation, and for molecules with more than 8–10

Received: August 31, 2020 Revised: October 29, 2020 Published: December 1, 2020





electrons. it is beyond the scope of traditional quantumchemical approaches. Determination of the precise energy and wave function of the |1TT| requires including configuration interaction (CI) with at least the dominant quadruple excitations from the HF ground state. We have theoretically investigated the | TT | using such high order CI in pentacene crystals,28 as well as covalently linked bipentacenes (BPn),²⁹ pentacene-tetracene heterodimers (PTn),³⁰ and the para- and meta-bisethynylpentacenylbenzene dimers (hereafter p- and m-Pc2)³¹ (see Figure S1 of Supporting Information for the chemical structures of the four dimers). We showed that with the exception of m-Pc2 in all other cases |1TT| should exhibit excited state absorptions (ESAs) in the near-infrared (NIR) and mid-IR, in addition to ESAs in the visible expected from free triplets. These theoretical predictions have been confirmed from TA measurements in pentacene crystals^{32–34} and BPn^{23,26} (see also discussion of p-Pc2 in ref 31), confirming the long lifetimes of $|^{1}TT\rangle$ in these systems. In m-Pc2, TA from $|^{1}TT\rangle$ in the IR is neither expected theoretically³¹ nor seen experimentally.⁷ Free triplet generation in m-Pc2 is likely, in agreement with the theoretically predicted weak binding energy of the I¹TT). 31,35

The ESAs from $|^1\text{TT}\rangle$ in the IR are due to intermonomer charge-transfer (CT) excitations. $^{28-31}$ CT from $|S_0S_1\rangle$, real or virtual, drives the transition to $|^1\text{TT}\rangle$, while the extent of CT contribution to $|^1\text{TT}\rangle$ determines the binding energy E_b of the $|^1\text{TT}\rangle$ (defined as $E_b = 2 \times E|S_0T_1\rangle - E|^1\text{TT}\rangle$, where $E|\cdots\rangle$ is the energy of the state being referred to). Since the magnitude of E_b determines the rate of $|^1\text{TT}\rangle$ dissociation, it follows that full many-body understanding of the role of CT in $|S_0S_1\rangle$ and $|^1\text{TT}\rangle$ will give qualitative understanding of the relationships between steps 1 and 2 of SF, if any. This is the goal of the present work.

Among iSF chromophores, the first step of SF is extremely rapid in p-Pc2, but E_b here is moderate to large, while m-Pc2 is almost at the other extreme with slow internal conversion but small E_b . We expect therefore that further study of para- and meta-linked chromophores will give deeper "global" insight into the two steps in SF. We have therefore performed calculations of many-body wave functions of hypothetical phenylene-linked p- and m-bianthracenes (hereafter p-2 and m-2) shown in Figure 1.

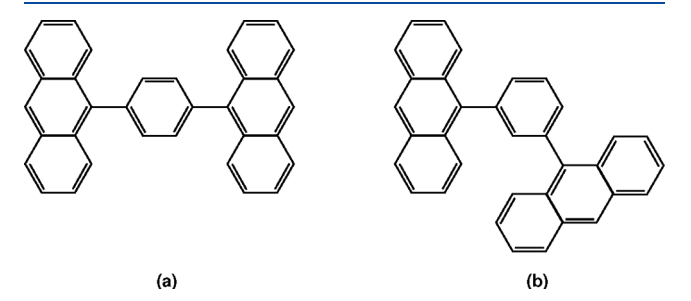


Figure 1. Hypothetical (a) p- and (b) m-bianthracene molecules.

We recognize at the outset that the compounds of Figure 1 do not exist currently and also that the real molecules will be nonplanar, unlike the planar dimer molecules investigated earlier. The advantage of calculations based on these model planar molecules is that the active space we are able to retain (24 MOs, see Figure 2) constitutes a very large fraction of the total number of π -orbitals (38). The correlated-electron wave functions that we obtain, including that of $|^{1}TT\rangle$, are

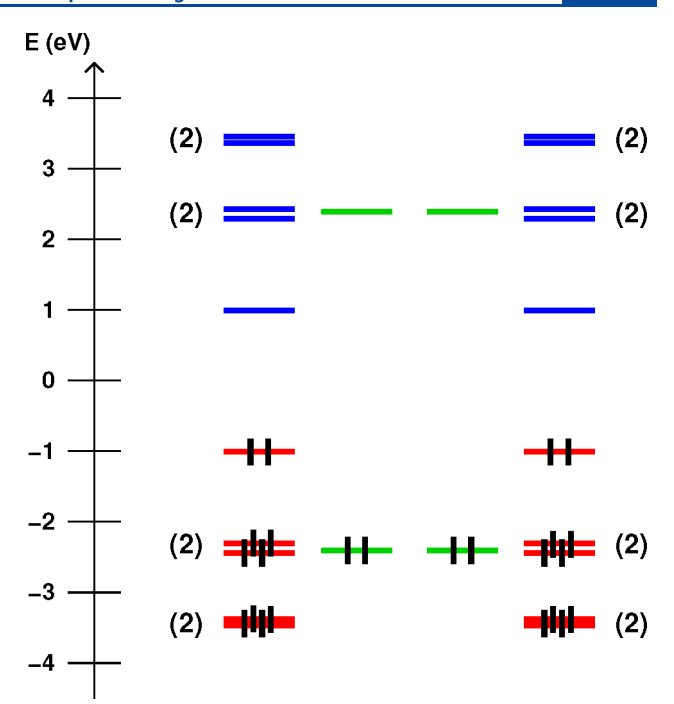


Figure 2. Huckel MOs localized on the individual anthracene molecules and the phenylene linker in the bianthracenes that constitute the active space for the PPP-MRSDCI calculations. Red and blue horizontal lines correspond to bonding and antibonding MOs of the anthracenes, while the green horizontal lines correspond to the doubly degenerate HOMOs and LUMOs of benzene. The numbers in parentheses give the number of close-lying MOs. The *y*-axis gives the energy with our hopping integrals.

therefore near-exact within our model. We show that these near-exact wave functions, in spite of the small sizes of the model systems, provide very clear understanding of not only the experimental differences between *p*-Pc2 and *m*-Pc2, but that the physical understanding reached can be extended to other iSF systems (BPn and PTn) that we had investigated before. On the basis of our analysis of wave functions, we argue that the yield of free triplets may be greater in SF systems with relatively slower dynamics, and vice versa. Although rapid annihilation of the |¹TT⟩ characterizes the bulk of the iSF materials, free triplets in bulk amounts have been observed in a limited number of materials. We discuss these experimental observations in Discussions and Conclusion within the context of our theory.

■ THEORETICAL MODEL, COMPUTATIONAL METHODS, AND PARAMETRIZATION

Model Hamiltonian. Our work is based on the π -electron only Pariser–Parr–Pople (PPP) Hamiltonian, 36,37

$$H = \sum_{\langle ij \rangle, \sigma} t_{ij} (c_{i\sigma}^{\dagger} c_{j\sigma} + c_{j\sigma}^{\dagger} c_{i\sigma}) + U \sum_{i} n_{i\uparrow} n_{i\downarrow}$$

$$+ \sum_{i < j} V_{ij} (n_{i} - 1)(n_{j} - 1)$$

$$(1)$$

where $c_{i\sigma}^{\dagger}$ creates an electron with spin σ on the p_z orbital of carbon (C) atom i, $n_{i\sigma} = \sum c_{i\sigma}^{\dagger} c_{i\sigma}$ is the number of electrons with spin σ on atom i, and $n_i = \sum_{\sigma} n_{i\sigma}$ is the total number of electrons on the atom. We retain electronic hoppings t_{ij} only between nearest neighbor carbon (C) atoms i and j. U is the Coulomb repulsion between two electrons occupying the p_z

orbital of the same C atom, and V_{ij} is long-range Coulomb interaction.

Our choice of the semiempirical PPP model over firstprinciples approaches is based on the need to include electron correlations to high order. The apparent disadvantages of semiempirical models are well-known: (i) the parameters entering the calculations can appear to be arbitrary; (ii) geometries of the molecules and bond lengths usually have to be assumed; and (iii) it is difficult to include electron-molecular vibration interactions accurately enough to account for differences in excited state and ground state geometries. Nevertheless, the semiempirical model remains the only choice when dynamic correlations have to be taken into account to high order, in order to determine ¹TT energy and wave function at the same level of accuracy as S1 and T1 energies and wave functions. As was shown by Tavan and Schulten many years ago in the context of linear polyenes, even though the ¹TT (2¹A_o) is predominantly a two electrontwo hole (2e-2h) excitation, CI including up to 4e-4h quadruples is essential for obtaining the correct relative energy of this state vis a vis the S_1 ($\tilde{1}^1B_u$) state in polyenes with 10 or more π -electrons.³⁸ This is because, (a) 2e-2h excitations are coupled by the many-electron interactions in eq 1 to the 4e-4h interactions, and (b) even as the relative weight of any individual 4e-4h configuration to the ¹TT is small, the number of 4e-4h configurations that contribute to the ${}^{1}TT$ increases rapidly with the number of π -electrons. The PPP model allows us to perform multiple reference single and double CI (MRSDCI) calculations, 39 which retain the dominant 4e-4h excitations for target eigenstates. Note also that the consequences of electron-vibration interactions can often be guessed from the calculations of bond orders in the excited states within the PPP model.41

MRSDCI. Unlike in our previous work, where we calculated ESAs from target states, 28-31 here we are interested only in the energies and wave functions of the latter and the ground state absorption. The computations are thus simpler and more accurate.³⁹ For each target excited state, we choose a trial set of appropriate 1e-1h and 2e-2h excitations from the single particle self-consistent MO "ground state" (see below) that best describe the target state. A double CI calculation is performed using these trial configurations, thereby generating the N_{ref} reference configurations that make significant contributions to the target state. At the next step a higher order CI calculation that includes up to double excitations from the N_{ref} reference configurations is performed. This generates both 3e-3h and 4e-4h excitations, as well as new 1e-1h and 2e-2h excitations coupled to these higher order excitations by the many-electron interactions in eq 1. The new 1e-1h and 2e-2h excitations along with the original 1e-1h and 2e-2h configurations form the next set of N_{ref} reference configurations and the procedure is repeated until convergence is reached. Convergence here is defined by the inclusion of the most dominant ne-nh (n = 1, 2, 3, 4) configurations in the normalized wave functions of targeted excited states, with coefficient \geq 0.04. Typically, convergence requires N_{ref} on the order of a few hundred and N_{total} several times 106.

Molecular Exciton Basis. Our goal is physical interpretation of all eigenstates, and to this end, it is desirable to distinguish not only between predominantly 1e—1h versus predominantly 2e—2h excitations but also between predominantly intraunit versus interunit excitations (where by

unit we refer to the individual anthracene monomers and the phenylene linker in Figure 1). Within the molecular exciton basis, the one-electron MO basis consists of simply the products of the MOs on the three individual units (see Figure 2). While a similar approach has also been used by others for calculations of SF, ^{2,10,41-43} these other calculations usually retain only the highest occupied and lowest unoccupied MO (HOMO and LUMO) of the individual units and a handful (usually between 5 and 10) of many-electron configurations. Our basis space exceeds 10⁶ for each targeted wave function.

We rewrite Hamiltonian 1 as $H_{intra} + H_{inter}$, where H_{intra} describes each individual unit, and H_{inter} consists of interunit t_{ij} and components of V_{ij} where atoms i and j belong to different units. Hintra are first solved separately for each unit within the Hartree-Fock (HF) approach, and the solution simply consists of products of HF MOs of the individual units (as in Figure 2). The basis functions for the complete Hamiltonian H_{intra} + H_{inter} are many-electron configurations with all possible electron occupancies of the localized MOs of Figure 2 including up to 4e-4h excitations from the "ground state" configuration that has all bonding MOs in Figure 2 fully occupied. The basis space for the different target states we have investigated are in all cases several million within the MRSDCI approach (see Supporting Information, Section C). In what follows, we show for each correlated wave function only the most dominant configurations that have the largest relative weights, along with their normalized CI coefficients. Because of the complex natures of the correlated wave functions in bianthracene to which the linker MOs make significant contributions, we explain here our notation by listing explicit examples of a select set of the diagrammatic many-electron basis configurations in Figure 3. In all cases we

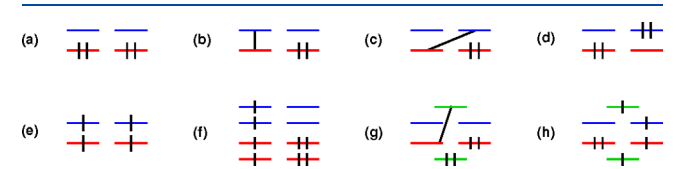


Figure 3. Sample S=0 diagrammatic basis functions. Bonding (antibonding) MOs absent in any diagram are completely filled (unoccupied). Lines connecting MOs represent singlet bonds. (a) The "ground state" configuration **G.** (b) One of two Frenkel excitations **FE.** (c) One of two configurations **CT** with charge-transfer between anthracene units. (d) One of two configurations **D** with doubly excited anthracene monomers. (e) Double excitation **TT** with 1e–1h excitations on both monomers; **TT** can be both spin singlet (S=0) and spin quintet (S=2). (f) Double excitations involving multiple bonding and antibonding MOs on anthracene units. (g) Configurations with charge-transfer between anthracene monomer and the phenylene linker; only the delocalized benzene MOs are shown (see text). (h) Double excitation involving anthracene and phenylene linker.

show the HOMO and LUMO of the individual anthracene MOs and their occupancies. MOs excluded in any diagram have the same occupancies as in Figure 2, viz., the excluded bonding (antibonding) MOs are completely occupied (unoccupied). The absence of the linker phenylene MOs in any configuration therefore indicates that they are "inactive" in that particular configuration. Configurations in which the phenylene linker MOs do participate in the excitations in bianthracene are also included in Figure 3. Only one each of

(a)
$$S_0S_0(p-2) = \begin{cases} 0.826 & \frac{1}{11} & \frac{1}{11} - 0.118 \left(\frac{1}{11} & \frac{1}{11} + \frac{1}{11} + \frac{1}{11} \right) + 0.081 \left(\frac{1}{11} & \frac{1}{11} + \frac{1}$$

(b)
$$S_0S_0(m-2) = \begin{cases} 0.832 \frac{1}{11} - 0.119 \left(\frac{1}{11} + \frac{11}{11} + \frac{11}{11}\right) + 0.081 \left(\frac{1}{11} + \frac{1}{11} + \frac{1}{11}\right) + 0.081 \left(\frac{1}{11} + \frac{1}{11} + \frac{1}{11}\right) + 0.081 \left(\frac{1}{11} + \frac{1}{11} + \frac{1}{11}\right) + 0.084 \left(\frac{1}{11} + \frac{1}{11}\right) \end{cases}$$

Figure 4. The near-exact normalized ground state wave functions (a) p-2 and (b) m-2. Note the relatively strong contributions by D and other intramonomer multiple excitations, but the absence of TT.

the doubly degenerate HOMO and LUMO of the benzene molecule is delocalized over the entire molecule, 44 and only these delocalized MOs participate in interunit charge-transfer. Hence, in the diagrammatic representations of configurations involving charge-transfer between anthracene and phenylene, only a single bonding or antibonding benzene MO is included. Note that participation by the localized benzene MO in configurations with intraphenylene excitations are however not precluded. Lines linking singly excited MOs in Figure 3 are spin-singlet bonds; these lines are replaced by arrows to describe spin-triplet bonds. We have not drawn bonds linking MOs in the case of double excitations. It is implied in the total spin S = 0 case that each such diagrammatic double excitation includes all three S_z components (+1 -1, 0 0, and -1 +1) where S_z is the zcomponent of the total spin.

Parametrization. We have chosen peripheral and internal bond lengths for the anthracene monomers to be 1.40 Å and 1.46 Å, 30 respectively, and the corresponding t_{ij} as -2.4 and -2.2 eV, respectively. 45 Both p-2 and m-2 are assumed to be planar, with bond lengths 1.40 Å and $t_{ij} = -2.4$ eV for the C–C bonds internal to the phenylene linker and bond length 1.46 Å and -2.2 eV, respectively, for the interunit bonds between the anthracene monomers and the phenylene linker. We use the screened Ohno parametrization for the longrange Coulomb repulsion, $V_{ij} = U/\kappa \sqrt{1 + 0.6117R_{ij}^2}$, where R_{ij} is the distance in Å between C atoms i and j and k is an effective dielectric constant. 46 The Coulomb parameter U (7.7 eV) and the dielectric constant κ (1.3) are chosen by quantitative fitting of the anthracene monomer singlet and triplet excitation energies (see Supporting Information).

■ RESULTS AND ANALYSIS

In the following, we present the results of our computations on p-2 and m-2, comparing these against our previous computational results for pentacene dimers²⁹⁻³¹ wherever appropriate. We find that in spite of the greater contribution of the linker MOs to the wave functions of p-2 and m-2, theory finds that the fundamental photophysics are the same for our model molecules and the larger systems.

The Ground States of p-2 and m-2. We have given in Figure 4 the most dominant components of the correlated ground states of p-2 and m-2 for U = 7.7 eV, $\kappa = 1.3$. Our most important conclusions are that (i) the relative weight of G, as measured by the square of its CI coefficient, in the near-exact $|S_0S_0\rangle$ eigenstates of parts a and b of Figures 4 is only about 65%, (ii) $|S_0S_0\rangle$ has small but nonzero contribution from D but a vanishingly small contribution from TT, and (iii) somewhat surprisingly, the ground state wave functions of these differently linked dimer molecules are practically identical. The strong admixing of configurations in $|S_0S_0\rangle$ (in particular the relatively small contribution by **G**), which is separated from $|S_0S_1\rangle$ and $|^1TT\rangle$ by large energy gaps, clearly indicates the futility of trying to guess the behavior of the |1TT > , which is proximate to other eigenstates, from the character of TT alone.

Excited State Energies. In Table 1, we have given the excited state energies of $|S_0S_1\rangle$, $|S_0T_1\rangle$, and the spin-singlet

Table 1. Excited State Energies (in eV) of p-2 and m-2, along with their spin gaps Δ_S and binding energy E_b^a

Compound	S_0S_1	S_0T_1	^{1}TT	⁵ TT	Δ_S	E_b	
p-2	2.81	1.68	2.97	3.51	0.53	0.38	
m-2	3.03	1.73	3.43	3.42	-0.01	0.03	
${}^{a}\Delta_{S} > E_{b}$ in p -2 is a finite size effect. 31							

and spin-quintet triplet—triplets $|^1\mathrm{TT}\rangle$ and $|^5\mathrm{TT}\rangle$ for p-2 and m-2. We have also included the spin-gap $\Delta_S = E(|^5\mathrm{TT}\rangle) - E(|^1\mathrm{TT}\rangle)$ and E_b . The significant differences between the energies of the optical singlet state and of the triplet exciton in the monomer versus the dimer indicate greater delocalization in p-2 and m-2, compared to BPn, 29 PTn, 30 and p- and m-Pc2; 31 the monomer versus dimer energy differences are vanishingly small in dimers of the larger acenes. The larger delocalization in p-2 and m-2 is, however, between anthracene monomers and the phenylene linker and not between the anthracene monomers themselves (see below). The very small Δ_S and E_b values in Table 1 for m-2 are completely in agreement with what was previously obtained in m-Pc2, 31 which is surprising, given the apparently delocalized nature of $|^1\text{TT}\rangle$ here. This is the first sign that

Figure 5. Optical spin-singlet wave functions of (a) p-2 and (b) m-2.

(a)
$$S_0T_1(p-2) = \begin{cases} 0.527 \left(- \underbrace{\uparrow}_{++} + \underbrace{\downarrow}_{++} + \underbrace{\downarrow}_{++} \right) + 0.101 \left(\underbrace{\downarrow}_{++} - \underbrace{\downarrow}_{++} \right) + 0.141 \left(\underbrace{\downarrow}_{++} + \underbrace{\downarrow}_{++} + \underbrace{\downarrow}_{++} + \underbrace{\downarrow}_{++} \right) - 0.127 \underbrace{\downarrow}_{++} + \underbrace{\downarrow}_{++} + \underbrace{\downarrow}_{++} + \underbrace{\downarrow}_{++} + \underbrace{\downarrow}_{++} + \underbrace{\downarrow}_{++} + \underbrace{\downarrow}_{++} \right) - 0.102 \left(\underbrace{\downarrow}_{++} + \underbrace{\downarrow}_{++} + \underbrace{\downarrow}_{++} + \underbrace{\downarrow}_{++} + \underbrace{\downarrow}_{++} + \underbrace{\downarrow}_{++} + \underbrace{\downarrow}_{++} \right) - 0.102 \left(\underbrace{\downarrow}_{++} + \underbrace{\downarrow}_{++} +$$

(b)
$$S_0T_1(m-2) = \begin{cases} 0.621 & \boxed{1} & \boxed{1} & 0.490 & \boxed{1} & \boxed{1} & 0.098 & \boxed{1} & \boxed{1} & 0.089 &$$

Figure 6. Lowest spin triplet wave functions of (a) p-2 and (b) m-2. The arrows designate spin-triplet bonds, inclusive of all three S_z components. The labels "T" on the double excitations indicate that the configurations have total spin S = 1.

$$(a) \ ^{1}TT(p-2) = \left\{ \begin{array}{c} 0.494 \stackrel{+}{+} \stackrel{+}{+} + 0.276 \left(\stackrel{+}{+} \stackrel{+}{+} \stackrel{+}{+} \stackrel{+}{+} - \stackrel{+}{+} \stackrel{+}{+} \stackrel{+}{+} - \stackrel{+}{+} \stackrel{+}{+} \stackrel{+}{+} - \stackrel{+}{+} \stackrel{+}{+} \stackrel{+}{+} \stackrel{+}{+} - \stackrel{+}{+} \stackrel{+}{+$$

(b)
$${}^{5}TT(p-2) = \begin{cases} 0.775 \stackrel{+}{+} \stackrel{+}{+} + 0.125 \begin{pmatrix} \stackrel{+}{+} \stackrel{+}{+} - \stackrel{+}{+} \stackrel{+}{+} \end{pmatrix} + 0.094 \begin{pmatrix} \stackrel{+}{+} \stackrel{+}{+} - \stackrel{+}{+} \stackrel{+}{+} \end{pmatrix} + 0.086 \begin{pmatrix} \stackrel{+}{+} \stackrel{+}{+} - \stackrel{+}{+} \stackrel{+}{+} \end{pmatrix} + 0.086 \begin{pmatrix} \stackrel{+}{+} \stackrel{+}{+} - \stackrel{+}{+} \stackrel{+}{+} + \stackrel{+}{+} \end{pmatrix} + 0.086 \begin{pmatrix} \stackrel{+}{+} \stackrel{+}{+} - \stackrel{+}{+} \stackrel{+}{+} \stackrel{+}{+} \end{pmatrix}$$

Figure 7. Normalized wave functions (a) $|^{1}TT\rangle$ and (b) $|^{5}TT\rangle$ of p-2. The dots represent multiple intervening MOs. Admixing with G and CT gives the nonzero binding energy of the S=0 spin-biexciton $|^{1}TT\rangle$.

delocalization into the linker molecule does not affect the relationships between the essential singlet, triplet, and triplet—triplet states and that conclusions based on

calculations on these model molecules can be extended to other dimers.

Singlet and Triplet Exciton Wave Functions. In Figure 5, we have shown the wave functions for $|S_0S_1\rangle$ in

Figure 8. Normalized wave functions (a) $|^{1}$ TT \rangle and (b) $|^{5}$ TT \rangle of m-2. The coefficients of individual configurations are the same in parts a and b, indicating that the wave functions are completely identical.

The $|S_0T_1\rangle$ states of p-2 and m-2, shown in Figure 6, are different from one another in the same way as the spin singlet states. The anthracene monomers are therefore nearly completely decoupled in $|S_0S_1\rangle$ and $|S_0T_1\rangle$ states of m-2. The contribution by CT, relative to the FE configuration, is significantly smaller in $|S_0T_1\rangle$ than $|S_0S_1\rangle$ of p-2, indicating that the lowest triplet is more localized than the optical singlet, a feature generally true with π -conjugated systems within correlated-electron models.

The Triplet-Triplet Spin-Biexcitons. In Figure 7, we have shown the $|^{1}TT\rangle$ and $|^{5}TT\rangle$ wave functions for p-2. Not surprisingly, TT makes the largest contribution to both wave functions, although the contributions are very different to the two spin states. Importantly, the contribution of D is nearly zero. As was found previously for stacks of polyenes, 48 there is nearly complete decoupling between double excitation within a single monomer versus double 1e-1h excitations on different acene monomers. The spin-singlet and quintet wave functions are very different in character. The strong contributions by G and CT to $|^{1}TT\rangle$ and their absence in $|^{5}TT\rangle$ are both expected, because of the overall spin S=0character of these configurations. The large Δ_S and E_b of p-2 (see Table 1) are also due to the strong contributions by G and CT to |1TT). With increased size of the acene monomer, the relative weights of configurations in which the linker MOs are involved decreases and that of TT increases.³¹

Figure 8 shows the $|^{1}TT\rangle$ and $|^{5}TT\rangle$ wave functions for m-2. The absence of CT in $|^{1}TT\rangle$ is expected, based on the

absence of the same in $|S_0S_1\rangle$ and $|S_0T_1\rangle$. Note, however, that this occurs in spite of the triplet—triplet states occurring above $|S_0S_1\rangle$, indicating that the Heisenberg spin-Hamiltonian description of eigenstates³⁵ is not a requirement for absence of CT. More importantly, we note the rather remarkable result that the $|^1TT\rangle$ and $|^5TT\rangle$ wave functions in m-2 are practically identical: the relative weights of each individual configuration in the two normalized wave functions are the same, which is of course a consequence and signature of the very weak coupling between the anthracene monomers. Returning to Figure 7, we also note that $|^5TT\rangle$ in p-2 is closely related to these eigenstates.

Given the results of Figure 8 we returned to our work in ref 31 and determined the accurate triplet—triplet wave functions for p-Pc2 and m-Pc2 to high order (see the Supporting Information, Figures S2 and S3). We have found that the identical natures of $|^1\text{TT}\rangle$ and $|^5\text{TT}\rangle$ wave functions are true even for the real dimer m-Pc2. The spin-biexcitons occur energetically below $|S_0S_1\rangle$ in m-Pc2, and the wave functions are almost entirely superpositions of TT and higher energy 2e-2h excitations on the anthracene monomers. The linker MOs are largely inactive. As with m-2, the relative weights of each individual configuration is the same in both spin states of m-Pc2. This is in contrast to the $|^1\text{TT}\rangle$ and $|^5\text{TT}\rangle$ wave functions of p-Pc2, which are again different from one another.

DISCUSSIONS AND CONCLUSION

The very large active space we have used for correlated-electron calculations on p-2 and m-2 gives us confidence about the accuracy of the wave functions we obtain. In spite of greater linker MO contributions to the wave functions in these smaller molecules, we find that they give the correct information for the realistic dimers. The strong admixing of CT configurations in both $|S_0S_1\rangle$ and $|^1TT\rangle$ in p-2 and in the pentacene dimers BPn, PTn and p-Pc2 investigated previously indicates that SF in these systems is charge-transfer mediated. The relative weight of CT in $|S_0S_1\rangle$ in these cases directly controls the coupling between $|S_0S_1\rangle$ and

 $|^{1}TT\rangle$ and hence the time τ_{TT} in which the $|^{1}TT\rangle$ is formed $^{48-53}$ (we ignore here the requirement that the $|S_{0}S_{1}\rangle$ to | TT | transition must involve a symmetry-breaking interaction). To the best of our knowledge, there is currently no explicit discussion of the extent of CT mixing in $|^{1}TT\rangle$ and the consequence of such mixing. Our calculations for p-2 indicate that the relative weight of CT is significantly larger in $|^{1}TT\rangle$ than in $|S_{0}T_{1}\rangle$. The greater CT content of $|^{1}TT\rangle$ contributes to its lower energy relative to $2 \times E(|S_0T_1\rangle)$. We further note that CT contributions to energetically proximate $|S_0S_1\rangle$ and $|^1TT\rangle$ are comparable (see Figures 5a and 7a). This is simply a consequence of energy proximity $E(|S_0S_1\rangle) \simeq$ $E(|^{1}TT\rangle)$ within the correlated-electron Hamiltonian, which in turn is a requirement for efficient SF. Taken together, it follows that short τ_{TT} and moderate to large E_b go together. We note in this context that in m-2 we find CT content to be extremely small in $|S_0S_1\rangle$, $|^1TT\rangle$, and $|S_0T_1\rangle$. This would indicate both longer τ_{TT} and smaller E_b . We have gone through the previously obtained wave functions for BPn, PTn, p-Pc2, and m-Pc2, and we have found in all cases CT contributions to individual $|S_0S_1\rangle$ and $|^1TT\rangle$ are comparable, indicating that in all cases smaller au_{TT} is accompanied by larger E_b , and vice versa. Fast $|^{1}TT\rangle$ generation may therefore indicate that it does not further dissociate onto free triplets. In Table 2 we have given the calculated energies of the

Table 2. Calculated energies of the optical singlet and the triplet—triplet, the experimental time-constant of formation of the triplet—triplet (in ps) and the calculated binding energy of the latter for covalently-linked pentacene dimers^a

compound	$E S_0S_1\rangle$ (eV)	$E ^{1}TT\rangle$ (eV)	$ au_{\mathrm{TT}}$ (ps)	E_b (eV)
BP0	1.91	1.75	20^b	0.08
BP1	1.91	1.75	20 ^b	0.13
PT0	1.90, 2.17	1.97	0.83 ^c	0.09
PT1	1.91, 2.19	2.00	18.3°	0.06
p-Pc2	1.81	1.71	2.7 ± 1.0^{d}	0.08
m-Pc2	1.85	1 74	80^d	0.009

^aIn both PT0 and PT1 there are two optical singlet states. The calculated quantities are from refs 29 (BPn), 30 (PTn), and 31 (p-Pc2 and m-Pc2), respectively. ^bReference 6. ^cReference 7. ^dReference 12.

optical singlet and the triplet—triplet, along with the experimentally determined $\tau_{\rm TT}$ and our calculated E_b for BP0 and BP1, PT0, and PT1, and p-Pc2 and m-Pc2. A qualitative one-to-one correspondence between experimental $\tau_{\rm TT}^{-1}$ and calculated E_b is seen (the calculated E_b for BP1 is an outlier; the large error in the calculation is an indication that even an active space of 24 MOs is not sufficient for giving precise E_b here).

As pointed out in the Introduction, in most experiments with iSF compounds free triplets are not the end products in bulk amounts. Experiments that do detect free triplets appear to agree with our theoretically arrived at conclusion about the correspondence between short $\tau_{\rm TT}$ and small yield of free triplets, as we now point out.

(i) In recent experiments on ortho- and meta-linked phenylene-bridged pentacene dimers that are structurally different from the compounds we have investigated (see Figure S4 of the Supporting Information for the chemical structures), Sakai et al. have found that the rate constants for $|^{1}TT\rangle$ formation are 1.2×10^{11} s⁻¹ in the ortho- compound

and $2.1 \times 10^9 \text{ s}^{-1}$ in the meta-compound, respectively. ⁵⁴ The smaller rate constant in the meta-compound is clearly due to the weak contribution of CT to $|S_0S_1\rangle$, as found in our calculations for m-2 and m-Pc2. The quantum yields of $|^1\text{TT}\rangle$ in the two compounds are comparable. The authors performed time-resolved electron spin resonance on both systems, and concluded that the quantum yield of free triplets in the ortho-dimer with τ_{TT} 2 orders of magnitude faster is only 20%, in contrast to quantum yield greater than 100% in the meta-dimer. ⁵⁴ The comparable quantum yields of $|^1\text{TT}\rangle$ in the two compounds suggests that the loss in the ortho-dimer occurs in the second step of SF, presumably due to the larger E_b of $|^1\text{TT}\rangle$ here. Vanishing E_b in the meta-compound would be expected from our calculations.

- (ii) Copious yields of free triplets have been also obtained in a *nonconjugated* pentacene dimer ^{SS} (see Figure S4 of the Supporting Information for the chemical structure). Based on the absence of conjugation configuration, mixing between FE and CT, as well as between ¹TT and CT, is expected to be very weak here. Not surprisingly, the experimentally determined rate constant for $|^1$ TT \rangle formation (2.4 × 10 s⁻¹) is significantly smaller than that in most conjugated dimers, and it is comparable to the meta-linked pentacene dimer mentioned above. ^{S4}
- (iii) While our calculations are for iSF dimers, the conclusion regarding the correspondence between short $\tau_{\rm TT}$ and larger E_b is arrived at from noting the nearly comparable CT contents in $|S_0S_1\rangle$ and $|^1{\rm TT}\rangle$, and it should be equally true for xSF materials, where also the energies of these states are comparable. Pensack et al. have found precisely such a relationship in their measurements on amorphous pentacene nanoparticles with three different side groups. The authors find that although triplet—triplet quantum yield is independent of the size of the side group, $\tau_{\rm TT}$ increases with the size of the side group (as expected), and free triplet yield is highest in the nanoparticle with the longest $\tau_{\rm TT}$.

In conclusion, we calculated near-exact correlated wave functions of the optical singlet and triplet excitons, and the spin-singlet and quintet triplet-triplet biexcitons of hypothetical bianthracenes, p-2 and m-2, within the PPP Hamiltonian for realistic Coulomb correlations. The calculations reveal that with the exception of the ground state and 15TT), there is strong admixing of CT configurations in all eigenstates of p-2. Conversely, CT plays a very weak role in m-2, in which the $|^{1}TT\rangle$ and $|^{5}TT\rangle$ wave functions are identical. The identical characters of $|^{1}TT\rangle$ and $|^{5}TT\rangle$ are true for the real dimer m-Pc2. On the basis of the available experimental results 7 and our previous and current theoretical work, we suggest time-resolved electron spin resonance measurements in m-Pc2 to determine whether free triplets are being generated here too. Theoretical research on SF until now has largely concluded that it is mediated by chargetransfer. 2,41-43,49,50 Given the nature of the iSF compounds in which free triplets have been observed, 54,55 it is conceivable that charge-transfer plays a very weak role in these. Whether or not the direct mechanism of iSF¹⁰ is more relevant in compounds that have shown free triplet formation is an interesting theoretical question and a topic of future research.

ASSOCIATED CONTENT

5 Supporting Information

The Supporting Information is available free of charge at https://pubs.acs.org/doi/10.1021/acs.jpca.0c07938.

TIPS-acene dimers BP0, BP1, PT0, PT1, p-Pc2, and m-Pc2, linked by phenylene spacer groups, experimental and calculated singlet and triplet energies of anthracene, Hamiltonian matrix dimensions for ground state, optical singlet, triplet, and triplet—triplet states for p-2 and m-2, ¹TT and ⁵TT wave functions of pentacene dimers p-Pc2 and m-Pc2, and TIPS—pentacene dimers whose dynamics and free triplet yields have been investigated recently (PDF)

AUTHOR INFORMATION

Corresponding Author

Sumit Mazumdar — Department of Physics, Department of Chemistry and Biochemistry, and College of Optical Sciences, University of Arizona, Tucson, Arizona 85721, United States; ⊚ orcid.org/0000-0002-1010-4044; Email: mazumdar@email.arizona.edu

Authors

Rafi Chesler – Department of Physics, University of Arizona, Tucson, Arizona 85721, United States

Souratosh Khan – School of Information, University of Arizona, Tucson, Arizona 85721, United States

Complete contact information is available at: https://pubs.acs.org/10.1021/acs.jpca.0c07938

Notes

The authors declare no competing financial interest.

ACKNOWLEDGMENTS

S.M. is thankful to Professor Joseph Michl, University of Colorado, for the invitations to the summer workshops on singlet fission that allowed him to become aware of the advances being made in the field by research groups from all over the world. The authors are grateful to Professor Alok Shukla of Indian Institute of Technology, Bombay for significant help with computations. This research was supported by Grant NSF-CHE-1764152.

REFERENCES

- (1) Smith, M. B.; Michl, J. Singlet Fission. Chem. Rev. 2010, 110, 6891–6936.
- (2) Smith, M. B.; Michl, J. Recent Advances in Singlet Fission. *Annu. Rev. Phys. Chem.* **2013**, *64*, 361–386.
- (3) Lee, J.; Jadhav, P.; Baldo, M. A. High efficiency organic multilayer photodetectors based on singlet exciton fission. *Appl. Phys. Lett.* **2009**, 95, No. 033301.
- (4) Rao, A.; Wilson, M. W. B.; Hodgkiss, J. M.; Albert-Seifried, S.; Bässler, H.; Friend, R. H. Exciton Fission and Charge Generation via Triplet Excitons in Pentacene/ C_{60} Bilayers. *J. Am. Chem. Soc.* **2010**, 132, 12698–12703.
- (5) Congreve, D. N.; Lee, J.; Thompson, N. J.; Hontz, E.; Yost, S. R.; Reusswig, P. D.; Bahlke, M. E.; Reineke, S.; Van Voorhis, T.; Baldo, M. A. External Quantum Efficiency Above 100% in a Singlet-Exciton-Fission-Based Organic Photovoltaic Cell. *Science* **2013**, *340*, 334–337.
- (6) Sanders, S. N.; Kumarasamy, E.; Pun, A. B.; Trinh, M. T.; Choi, B.; Xia, J.; Taffet, E. J.; Low, J. Z.; Miller, J. R.; Roy, X.; et al. Quantitative Intramolecular Singlet Fission in Bipentacenes. *J. Am. Chem. Soc.* **2015**, *137*, 8965–8972.

- (7) Zirzlmeier, J.; Lehnherr, D.; Coto, P. B.; Chernick, E. T.; Casillas, R.; Basel, B. S.; Thoss, M.; Tykwinski, R. R.; Guldi, D. M. Singlet fission in pentacene dimers. *Proc. Natl. Acad. Sci. U. S. A.* **2015**, *112*, 5325–5330.
- (8) Lukman, S.; Musser, A. J.; Chen, K.; Athanasopoulos, S.; Yong, C. K.; Zeng, Z.; Ye, Q.; Chi, C.; Hodgkiss, J. M.; Wu, J.; et al. Tuneable Singlet Exciton Fission and Triplet-Triplet Annihilation in an Orthogonal Pentacene Dimer. *Adv. Funct. Mater.* **2015**, 25, 5452–5461.
- (9) Busby, E.; Xia, J.; Wu, Q.; Low, J. Z.; Song, R.; Miller, J. R.; Zhu, X.-Y.; Campos, L. M.; Sfeir, M. Y. A design strategy for intramolecular singlet fission mediated by charge-transfer states in donor-acceptor organic materials. *Nat. Mater.* **2015**, *14*, 426–433.
- (10) Fuemmeler, E. G.; Sanders, S. N.; Pun, A. B.; Kumarasamy, E.; Zeng, T.; Miyata, K.; Steigerwald, M. L.; Zhu, X. Y.; Sfeir, M. Y.; Campos, L. M.; et al. A Direct mechanism of Ultrafast Intramolecular Singlet Fission in Pentacene Dimers. *ACS Cent. Sci.* **2016**, 2, 316–324.
- (11) Sakuma, T.; Sakai, H.; Araki, Y.; Mori, T.; Wada, T.; Tkachenko, N.; Hasobe, T. Long-Lived Triplet Excited States of Bent-Shaped Pentacene Dimers by Intramolecular Singlet Fission. *J. Phys. Chem. A* **2016**, *120*, 1867–1875.
- (12) Sanders, S. N.; Kumarasamy, E.; Pun, A. B.; Steigerwald, M. L.; Sfeir, M. Y.; Campos, L. M. Intramolecular Singlet Fission in Oligoacene Heterodimers. *Angew. Chem., Int. Ed.* **2016**, *55*, 3373–3377
- (13) Sanders, S. N.; Kumarasamy, E.; Pun, A. B.; Appavoo, K.; Steigerwald, M. L.; Campos, L. M.; Sfeir, M. Y. Exciton Correlations in Intramolecular Singlet Fission. *J. Am. Chem. Soc.* **2016**, *138*, 7289–7297.
- (14) Korovina, N. V.; Das, S.; Nett, Z.; Feng, X.; Joy, J.; Haiges, R.; Krylov, A. I.; Bradforth, S. E.; Thompson, M. E. Singlet Fission in a Covalently Linked Cofacial Alkynyltetracene Dimer. *J. Am. Chem. Soc.* **2016**, *138*, 617–627.
- (15) Liu, H.; Nichols, V. M.; Shen, L.; Jahansouz, S.; Chen, Y.; Hanson, K. M.; Bardeen, C. J.; Li, X. Synthesis and photophysical properties of a face-to-face stacked tetracene dimer. *Phys. Chem. Chem. Phys.* **2015**, *17*, 6523–6531.
- (16) Margulies, E. A.; Miller, C. E.; Wu, Y.; Ma, L.; Schatz, G. C.; Young, R. M.; Wasielewski, M. R. Enabling singlet fission by controlling intramolecular π stacked covalent terrylenediimide dimers. *Nat. Chem.* **2016**, *8*, 1120–1125.
- (17) Korovina, N. V.; Chang, C. H.; Johnson, J. C. Spatial separation of triplet excitons drives endothermic singlet fission. *Nat. Chem.* **2020**, *12*, 391–398.
- (18) Pun, A. B.; Asadpoordarvish, A.; Kumarasamy, E.; Tayebjee, M. J. Y.; Niesner, D.; McCamey, D. R.; Sanders, S. N.; Campos, L. M.; Sfeir, M. Y. Ultra-fast intramolecular singlet fission to persistent multiexcitons by molecular design. *Nat. Chem.* **2019**, *11*, 821–828.
- (19) Weiss, L. R.; Bayliss, S. L.; Kraffert, F.; Thorley, K. J.; Anthony, J. E.; Bittl, R.; Friend, R. H.; Rao, A.; Greenham, N. C.; Behrends, J. Strongly exchange-coupled triplet pairs in an organic semiconductor. *Nat. Phys.* **2017**, *13*, 176–181.
- (20) Yong, C. K.; Musser, A. J.; Bayliss, S. L.; Lukman, S.; Tamura, H.; Bubnova, O.; Hallani, R. K.; Meneau, A.; Resel, R.; Maruyama, M.; et al. The entangled triplet pair state in acene and heteroacene materials. *Nat. Commun.* **2017**, *8*, 15953.
- (21) Stern, H. L.; Cheminal, A.; Yost, S. R.; Broch, K.; Bayliss, S. L.; Chen, K.; Tabachnyk, M.; Thorley, K.; Greenham, N.; Hodgkiss, J. M.; et al. Vibronically coherent ultrafast triplet-pair formation and subsequent thermally activated dissociation control efficient endothermic singlet fission. *Nat. Chem.* **2017**, *9*, 1205–1212.
- (22) Tayebjee, M. J. Y.; Sanders, S. N.; Kumarasamy, E.; Campos, L. M.; Sfeir, M. Y.; McCamey, D. R. Quintet multiexciton dynamics in singlet fission. *Nat. Phys.* **2017**, *13*, 182–188.
- (23) Trinh, M. T.; Pinkard, A.; Pun, A. B.; Sanders, S. N.; Kumarasamy, E.; Sfeir, M. Y.; Campos, L. M.; Roy, X.; Zhu, X.-Y. Distinct properties of the triplet pair state from singlet fission. *Science Advances* **2017**, *3*, No. e1700241.

- (24) Folie, B. D.; Haber, J. B.; Refaely-Abramson, S.; Neaton, J. B.; Ginsberg, N. S. Long-Lived Correlated Triplet Pairs in a π-Stacked Crystalline Pentacene Derivative. *J. Am. Chem. Soc.* **2018**, *140*, 2326–2335.
- (25) Pensack, R.; et al. Striking the right balance of intermolecular coupling for high-efficiency siglet fission. *Chem. Sci.* **2018**, *9*, 6240–6259.
- (26) Miyata, K.; Conrad-Burton, F. S.; Geyer, F. L.; Zhu, X.-Y. Triplet Pair States in Singlet Fission. *Chem. Rev.* **2019**, *119*, 4261–4292.
- (27) Musser, A. J.; Clark, J. Triplet-Pair States in Organic Semiconductors. *Annu. Rev. Phys. Chem.* **2019**, 70, 323–351.
- (28) Khan, S.; Mazumdar, S. Theory of Transient Excited State Absorptions in Pentacene and Derivatives: Triplet-Triplet Biexciton versus Free Triplets. J. Phys. Chem. Lett. 2017, 8, 5943–5948.
- (29) Khan, S.; Mazumdar, S. Diagrammatic Exciton Basis Theory of the Photophysics of Pentacene Dimers. *J. Phys. Chem. Lett.* **2017**, *8*, 4468–4478.
- (30) Khan, S.; Mazumdar, S. Optical probes of the quantumentangled triplet-triplet state in a heteroacene dimer. *Phys. Rev. B: Condens. Matter Mater. Phys.* **2018**, 98, 165202.
- (31) Khan, S.; Mazumdar, S. Free Triplets Versus Bound Triplet-Triplet Biexciton in Intramolecular Singlet Fission Materials: Structure-Property Correlations. *J. Phys. Chem. C* **2020**, *124*, 1171–1177.
- (32) Stuart, A. N.; Tapping, P. C.; Schrefl, E.; Huang, D. M.; Kee, T. W. Controlling the Efficiency of Singlet Fission in TIPS-Pentacene/Polymer Composite Nanoparticles. *J. Phys. Chem. C* **2019**, *123*, 5813–5825.
- (33) Zhou, Z.; Ma, L.; Guo, D.; Zhao, X.; Wang, C.; Lin, D.; Zhang, F.; Zhang, J.; Nie, Z. Ultrafast Dynamics of Long-Lived Bound Triplet Pair Generated by Singlet Fission in TIPS-Pentacene. *J. Phys. Chem. C* **2020**, *124*, 14503–14509.
- (34) Grieco, C.; Kennehan, E. R.; Kim, H.; Pensack, R. D.; Brigeman, A. N.; Rimshaw, A.; Payne, M. M.; Anthony, J. E.; Giebink, N. C.; Scholes, G. D.; et al. Direct Observation of Correlated Triplet Pair Dynamics during Singlet Fission Using Ultrafast Mid-IR Spectroscopy. *J. Phys. Chem. C* 2018, 122, 2012—2022.
- (35) Abraham, V.; Mayhall, N. J. Simple Rule To Predict Boundedness of Multiexciton States in Covalently Linked Singlet-Fission Dimers. J. Phys. Chem. Lett. 2017, 8, 5472–5478.
- (36) Pariser, R.; Parr, R. A Semi-Empirical theory of the electronic spectra and electronic structure of complex unsaturated molecules II. *J. Chem. Phys.* **1953**, *21*, 767–776.
- (37) Pople, J. A. Electron interaction in unsaturated hydrocarbons. *Trans. Faraday Soc.* **1953**, 49, 1375–1385.
- (38) Tavan, P.; Schulten, K. The 2^1A_g - 1^1B_u energy gap in the polyenes: An extended configuration interaction study. *J. Chem. Phys.* **1979**, *70*, 5407–5413.
- (39) Tavan, P.; Schulten, K. Electronic Excitations in Finite and Infinite Polyenes. *Phys. Rev. B: Condens. Matter Mater. Phys.* **1987**, 36, 4337–4358.
- (40) Goli, V. M. L. D. P.; Prodhan, S.; Mazumdar, S.; Ramasesha, S. Correlated electronic properties of some graphene nanoribbons: A DMRG study. *Phys. Rev. B: Condens. Matter Mater. Phys.* **2016**, *94*, No. 035139.
- (41) Japahuge, A.; Zeng, T. Theoretical Studies of Singlet Fission: Searching for Materials and Exploring Mechanisms. *ChemPlusChem* **2018**, 83, 146–182.
- (42) Casanova, D. Theoretical Modeling of Singlet Fission. *Chem. Rev.* 2018, 118, 7164–7207.
- (43) Tempelaar, R.; Reichman, D. R. Vibronic exciton theory of singlet fission. I. Linear absorption and the anatomy of the correlated triplet pair state. *J. Chem. Phys.* **2017**, *146*, 174703.
- (44) Salem, L. Molecular Orbital Theory of Conjugated Systems; Benjamin: New York, 1966.

- (45) Ducasse, I. R.; Miller, T. E.; Soos, Z. G. Correlated states in finite polyenes: Exact PPP results. *J. Chem. Phys.* **1982**, *76*, 4094–4104.
- (46) Chandross, M.; Mazumdar, S. Coulomb interactions and linear, nonlinear, and triplet absorption in poly(para-phenylenevinylene). *Phys. Rev. B: Condens. Matter Mater. Phys.* **1997**, *55*, 1497–1504.
- (47) Ito, S.; Nagami, T.; Nakano, M. Design Principles of Electronic Couplings for Intramolecular Singlet Fission in Covalently-Linked Systems. *J. Phys. Chem. A* **2016**, *120*, 6236–6241.
- (48) Aryanpour, K.; Shukla, A.; Mazumdar, S. Theory of Singlet Fission in Polyenes, Acene Crystals, and Covalently Linked Acene Dimers. *J. Phys. Chem. C* **2015**, *119*, 6966–6979.
- (49) Zeng, T.; Hoffmann, R.; Ananth, N. The Low-Lying Electronic States of Pentacene and Their Roles in Singlet Fission. J. Am. Chem. Soc. 2014, 136, 5755–5764.
- (50) Monahan, N.; Zhu, X.-Y. Charge Transfer-Mediated Singlet Fission. *Annu. Rev. Phys. Chem.* **2015**, *66*, 601–618.
- (51) Feng, X.; Krylov, A. I. On couplings and excimers: lessons from studies of singlet fission in covalently linked tetracene dimers. *Phys. Chem. Chem. Phys.* **2016**, *18*, 7751–7761.
- (52) Alvertis, A. M.; Lukman, S.; Hele, T. J. H.; Fuemmeler, E. G.; Feng, J.; Wu, J.; Greenham, N. C.; Chin, A. W.; Musser, A. J. Switching between Coherent and Incoherent Singlet Fission vis Solvent-Induced Symmetry Breaking. J. Am. Chem. Soc. 2019, 141, 17558–17570.
- (53) Chen, M.; Shin, J. Y.; Young, R. M.; Wasielewski, M. R. Tuning the charge-transfer character of the multiexcitons state in singlet fission. *J. Chem. Phys.* **2020**, *153*, No. 094302.
- (54) Sakai, H.; Inaya, R.; Nagashima, H.; Nakamura, S.; Kobori, Y.; Tkachenko, N. V.; Hasobe, T. Multiexciton dynamics depending on intramolecular orientations in pentacene dimers: Recombination and dissociation of correlated triplet pairs. *J. Phys. Chem. Lett.* **2018**, *9*, 3354–3360.
- (55) Basel, B. S.; Zirzlmeier, J.; Hetzer, C.; Phelan, B. T.; Krzyaniak, M. D.; Reddy, S. R.; Coto, P. B.; Horwitz, N. E.; Young, R. M.; White, F. J.; et al. Unified model for singlet fission within a non-conjugated covalent pentacene dimer. *Nat. Commun.* **2017**, *8*, 15171.